

**FIRST-PRINCIPLES DENSITY FUNCTIONAL THEORY STUDIES OF THE STRUCTURAL AND  
ELECTRONIC PROPERTIES OF PRODIGIOSIN AS A CANCER DRUG**

A Thesis Presented to the Department of Materials Science and Engineering  
African University of Science and Technology, Abuja in partial fulfilment of the requirements  
for the award of MASTER OF SCIENCE DEGREE

By

BILAU ABDULWAHEED ADEMOLA

Supervised by

Dr Nelson Y. Dzade



African University of Science and Technology [www.aust.edu.ng](http://www.aust.edu.ng)

P.M. B 681, Garki, Abuja F.C.T

Nigeria.

June, 2019

**FIRST-PRINCIPLES DENSITY FUNCTIONAL THEORY STUDIES OF THE STRUCTURAL AND  
ELECTRONIC PROPERTIES OF PRODIGIOSIN AS A CANCER DRUG**

By

BILAU ABDULWAHEED ADEMOLA

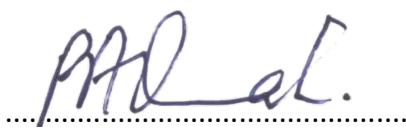
A THESIS APPROVED BY THE DEPARTMENT OF MATERIALS SCIENCE AND ENGINEERING

RECOMMENDED:



.....23<sup>rd</sup> May 2020.....

Supervisor: Dr Nelson Y. Dzade



.....  
Prof. Azikiwe Peter Onwualu

Head, Department of Materials Science and Engineering

APPROVED:

.....

Chief Academic Officer (Prof. C. E. Chidume)

.....

Date

## ABSTRACT

Prodigiosin molecule, whose efficacy in the treatment of cancer has proven positive, has been studied using first-principles Density Functional Theory (DFT) methods as implemented in VASP - Vienna Ab initio Simulation Package. Initial structure of prodigiosin generated using ArgusLab 4.0.1 program was subjected to geometry optimization in the VASP program in order to determine the ground state structure. The optimized interatomic bond lengths and angles are comprehensively characterized. Important properties such as the electrostatic potential (ESP) map, HOMO-LUMO iso-contours, Mulliken charges and solvent accessibility surface area were also characterized as determined in the ArgusLab 4.0.1 software.

The Mulliken charges calculated, predict the direction of delocalization of electrons in the molecule. Electrostatic potential map showed the areas of the molecule that would be susceptible to nucleophilic and electrophilic attack. As ESP predicts the most reactive part of the molecule, the chemical reactivity is also understood from its chemical potential, electrophilicity and hardness. HOMO-LUMO energy gap of the molecule also reflects the chemical reactivity, polarizability and chemical hardness of a molecule. Solvent accessibility surface area of the molecule gives better understanding on the contact surface of the molecule when used as drug in the aqueous environment such as in the human body.

Finally, this study will be helpful in drug design and drug delivery of prodigiosin for cancer treatment. It is also foreseen that studies could be done on polymerization of prodigiosin molecule as its conjugate bonding system may open a new frontier of research as a promising electrically conducting polymer.

## **ACKNOWLEDGEMENT**

My sincere gratitude goes to my supervisor, Dr Nelson Dzade of Cardiff University, UK, for his extraordinary effort towards the success of this work. He was both a mentor and a father.

To the Head of Department of Materials Science and Engineering, Prof. Peter Onwualu, he mentored us and his fatherly presence helped us succeed. I am also grateful to all the faculties of AUST, thank you for sharing knowledge in the best form.

To my sponsors, African University of Science and Technology (AUST), Pan-African Materials Institute (PAMI), World Bank, and Lagos State Government, I am indeed grateful.

My family members have been instrumental to the success of my programme and I will specially thank my sister, Adebola Kudirat. She is a wonderful sister.

It is very important that I mention some of my wonderful friends that were instrumental to the success of my studies. They are Ibrahim, Habib Olanrewaju, Ologun, Mojeed and Ahmed, Mustapha. A friend in need is a friend indeed. To all my colleagues at AUST, it was an honour being with you all. You all contributed to my success.

## **DEDICATION**

*This work is dedicated to Almighty Allah who has bestowed knowledge on mankind.*

*To my father, Sheu Adeoye for being a motivation for us.*

*To my mother, Anthonia Nkemjika for her love and care.*

*To my wife, Adetoun Tawakalt, for standing by me.*

*To my son, Ademola Abdurrahman, my joy.*

# CONTENTS

ABSTRACT	iii
ACKNOWLEDGEMENT	iv
DEDICATION	v
CONTENTS	vi
LIST OF ABBREVIATION	viii
LIST OF FIGURES	ix
LIST OF TABLES	x
CHAPTER ONE	1
INTRODUCTION	1
1.1 Background	1
1.2 Problem Statement	2
1.3 Aim and Objectives	3
CHAPTER TWO	4
LITERATURE REVIEW	4
2.1 Introduction	4
2.2 Prodigiosin Production by <i>Serratia marcescens</i>	5
2.2.1 Prodigiosin Structure	6
2.3 Density Functional Theory (DFT)	7
2.3.1 The Thomas-Fermi (TF) Model	10
2.3.1 The Hohenberg-Kohn (HK) Theorem	10
2.3.2 Wave-Function Based Methods	13
2.3.3 Exchange-correlation functional	13
2.3.4 The Local-Density Approximation (LDA)	14
2.3.5 The Generalized-Gradient Approximation (GGA)	15
2.3.6 Meta-GGA (mGGA)	17
2.3.7 Hybrid Schemes	18
2.3.1 Basis Sets	18
2.3.2 Plane Waves	19
2.4 Frontier Molecular Orbitals	21

2.4.1	HOMO-LUMO	22
2.5	Electrostatic Potential	23
2.6	Solvent Accessibility Surface Area	24
CHAPTER THREE		26
COMPUTATIONAL DETAILS		26
CHAPTER FOUR		27
RESULTS AND DISCUSSION		27
4.1	Optimized Molecular Structure of Prodigiosin and Geometry Parameters	27
4.2	Mulliken Atomic Charges	30
4.3	Frontier Molecular Orbital: HOMO and LUMO	31
4.4	Electrostatic Potential Map (ESP)	33
4.5	Solvent Accessibility Surface Area	34
CHAPTER FIVE		35
SUMMARY AND CONCLUSIONS		35
References		36

## LIST OF ABBREVIATION

CI - Configuration Interaction

DFT - Density-Functional Theory

ESP - Electrostatic Potential

xc - Exchange–Correlation

GEA - Gradient–Expansion Approximation

GGA - Generalized–Gradient Approximation

HF - Hartree–Fock

HK - Hohenberg–Kohn

HOMO - Highest Occupied Molecular Orbital

HS - Hanke and Sham

KS - Kohn–Sham

LDA - Local Density Approximation

LUMO - Lowest Unoccupied Molecular Orbital

mGGA - Meta-GGA

TF - Thomas-Fermi



## LIST OF FIGURES

FIGURE 4. 1: OPTIMIZED GEOMETRY OF PRODIGIOSIN MOLECULE. COLOUR CODE: CARBON = RED, OXYGEN = RED, NITROGEN = BLUE, HYDROGEN = WHITE.	27
FIGURE 4. 2: HIGHEST OCCUPIED MOLECULAR ORBITAL DIAGRAM OF PRODIGIOSIN	32
FIGURE 4. 3: LOWEST UNOCCUPIED MOLECULAR ORBITAL DIAGRAM OF PRODIGIOSIN	32
FIGURE 4. 4: ELECTROSTATIC POTENTIAL-MAPPED ELECTRON DENSITY SURFACE OF PRODIGIOSIN	33
FIGURE 4. 5: SOLVENT ACCESSIBILITY SURFACE AREA OF PRODIGIOSIN	34

## LIST OF TABLES

TABLE 4. 1: GEOMETRY OPTIMIZED INTERATOMIC BOND DISTANCES IN PRODIGIOSIN	28
TABLE 4. 2: GEOMETRY OPTIMIZED BOND ANGLES IN PRODIGIOSIN	29
TABLE 4. 3: MULLIKEN ATOMIC CHARGES OF PRODIGIOSIN	30

# CHAPTER ONE

## INTRODUCTION

### 1.1 Background

Cancer is a medical condition broadly used in defining over 200 human diseases [1]. The increasing incidence of cancer [1] has stimulated research on the development of novel therapies that would be effective in the treatment and reduction in the rate of re-occurrence. Recent findings show that cancer is the second leading cause of death while cardiovascular diseases are on top of the list [2]. Among the 200 different classes of diseases, breast cancer is the second most common cause of cancer death in women. It is projected that cancer will be the leading cause of death by 2030 as seen trend studies [3].

Abnormal genetic changes which occur in genes cause one cell or a few cells to proliferate and multiply in an uncontrolled manner leading to formation of cancer cells. Cancer usually starts as mild tumour which is known to be the primary stage and if not arrested, it spreads to other healthy cells which is termed as the secondary stage or metastasis [1]. Generally, cancer treatment procedures have adverse effects on the body systems, such as blood circulation, lymphatic and immune systems, and the hormone system problems [2]. Common treatments methods for cancer include surgical means, chemotherapy, targeted therapy, immune therapy, radiation etc [1].

It is believed that cancer is caused both by external factors which include cigarette smoking, infections, poor diet, as well as internal factors, such as in hereditary, hormone imbalance, and poor immune system.

*Serratia marcescens* is a gram-negative bacillus, which belongs to the family Enterobacteriaceae [1]. It is an omnipresent bacterium inhabiting in both terrestrial and aquatic habitat. One of its major characteristics that interests us in this study is its ability to produce pigments known as Prodigiosin. Prodigiosin accelerates the process of apoptosis in cancerous cells. This is a form of caspase-mediated cell death in which cells actively participate in their own destruction [4].

## 1.2 Problem Statement

Designing a drug for cancer treatment basically involves optimisation of small molecules aimed at having requisite diagnostic features. Some of the information can be obtained experimentally, however, the process is lengthy, financially costly and has a very low success rate in identifying potential lead compounds [5] [6].<sup>refs</sup> As a way to combat these challenges, molecular modelling tools, for example, first-principles density functional theory (DFT) calculations and molecular dynamics (MD) simulations can be incorporated in research to get the much valuable information necessary for designing drug molecules in a timeous and less costly way. Accurate atomistic first-principles DFT calculations carried out on high-performance computers can significantly reduce the number of time-consuming laboratory experiments required to test the efficacy of prodigiosin, its electronic properties etc., hence predictive modelling and simulations offer the most intelligent and efficient path forward to significantly expand the parameter space whilst lowering both costs and development times. DFT methods have become one of the most popular and successful Quantum Mechanics (QM) approach for large systems. Currently, DFT has experienced wide applications for “*ab initio*” calculations of the structure of atoms, molecules, crystals, surfaces and their interactions [7]. It is nowadays routinely applied for calculating e.g., the binding energy of molecules in

chemistry and the band structure of solids in physics. First application relevant for fields traditionally considered more distant from quantum mechanics, such as biology and mineralogy are beginning to appear [7].

### **1.3 Aim and Objectives**

This thesis aims to presents a theoretical study that provides new insights into the structural and electronic properties of prodigiosin, a promising drug reported for its characteristics of having antifungal, immune-suppressive, anti-malaria and antiproliferation activity of cancer cells in human. Below are the objectives of the current work.

1. To develop the molecular structure of Prodigiosin and characterise the geometric parameters (interatomic bond distances and angles)
2. Comprehensively characterise the electronic properties such as atomic charges, lowest unoccupied molecular orbital (LUMO) and highest occupied molecular orbital (HOMO), electrostatic potential (ESP) and Solvent accessible surface.

## CHAPTER TWO

### LITERATURE REVIEW

#### 2.1 Introduction

Prodigiosin is a macromolecule which belongs to the family of a natural red pigment commonly characterized by a pyrrolylpyrromethene skeleton, are produced by various bacteria which was first characterized from *Serratia marcescens* [8]. It is a pigment and a promising drug owing to its repeated characteristics of having antifungal, immunosuppressive and antiproliferative activity [1]. Prodigiosin can also induce apoptosis in human cancer cell lines [8]. For targeted delivery of anticancer drugs, several receptors, which are over-expressed in cancer cells, are selected targets for polymer binding, such as prostate specific membrane antigen (PSMA), epidermal growth factor receptor (EGFR), and Luteinizing-hormone-releasing hormone (LHRH) receptor [1]. LHRH is an amino acid peptide hormone secreted by the hypothalamus and it also regulates gametogenesis. Effects of the overexpression of LHRH receptors are seen in prostate (86%), ovarian (80%), and breast (50%) cancers and have low expression in healthy organs [9].

Recently, LHRH and its analog have been used in the clinical trial in the management of prostate cancer. Active targeting by LHRH is expected to be safe and efficient after systemic administration. Due to the short half-life of natural LHRH, synthetic LHRH analog with improved bioactivity has been widely used for targeting LHRH-receptors [2].

Of the various approaches to target cancer therapy, one is based on findings that receptors for certain peptide hormones such as somatostatin, bombesin, and LHRH are expressed on tumours in higher concentrations than on most normal cells [1]. As such, analogs of these

peptide hormones can be used as carrier vectors for direct delivery of cytotoxic agents to cancerous cells. This increases the concentration of the drugs in tumour tissue and sparing normal, noncancerous cells from exposure which are not necessary [3].

## **2.2 Prodigiosin Production by *Serratia marcescens***

*Serratia marcescens* a family of Enterobacteriaceae is a gram-negative bacterium [1]. These bacteria can produce three special enzymes such as DNAase, lipase, and gelatinase. As a result of these characteristics, it has made them different from other genera of bacteria. But there are a number of other characteristics that have been seen in this species that may influence their pathogenesis [1]. These characteristics include swarming and swimming, motility and extracellular enzyme activities; i.e. nuclease, protease, and haemolysin [10]. *Serratia marcescens* can occur in water, soil, on plants, in insects, man and in animals [10]. It is the only pathogen of the genera while others such as *S. plymuthica*, *liquefaciens*, *rubidaea* and *odifera* are organism causing diseases. It produces prodigiosin which is a secondary metabolite [1].

Prodigiosin is naturally produced and it represents one of the critical sources of chemical diversity and potential medicinal use [11]. The production of prodigiosin by *Serratia marcescens* is a recall of its secondary metabolism commonly referred to as bio-pigments. The bio-pigments produced have a vast synthetic and commercial applications [11]. Pigment varies among different species and it depends on many factors such as species type and incubation time [12]. The variation also depends on species habitats. Terrestrial species found in soil especially dump sites, had the incubation time ranging from 24h to 72 h. There is no defined role for these pigments in the physiology of producing strains but reports have it to have antifungal, antibacterial, algicidal, antiprotozoal, antimalarial activities, immune-

suppressive, and anticancer activities [13]. The culture media used for prodigiosin biosynthesis are nutrient broth and peptone glycerol agar [1]. Powdered l-peanuts medium showed forty-fold increase in the concentration of prodigiosin [2].

Many factors contribute to the anticancer and immune-suppressive activity of prodigiosin. In Prodigiosin structure analogs have been designed and also the ring of pyrrole has also been reported to be very important in activity in therapeutic applications. Mekheal and Yousif in 2009 reported that purified prodigiosin showed plasmid curing activity on plasmids of *E. coli* HB101 and *S. aureus* [14].

### **2.2.1 Prodigiosin Structure**

Prodigiosin is a family of tri-pyrrole red pigments that contains a common 4-methoxy, 2-2 bipyrrrole ring system. The biosynthesis of the pigment is a bifurcated process in which mono and bipyrrrole precursors are synthesized separately and then assembled to form prodigiosin [15]. Studies has shown that prodigiosin is associated with extracellular vesicles, and cells associated or present in intracellular granules [12]. It has a chemical formula of  $C_{20}H_{25}N_3O$  and a molecular weight of 323.44 Da. It is sensitive to light and insoluble in water. Its solubility is moderate in alcohol and ether, and soluble in chloroform, methanol and acetonitrile.

### **2.2.2 Effects of Growth Conditions on Yield of Prodigiosin**

*Serratia* species, like other Enterobacteriaceae, thrive well on ordinary media under anaerobic and aerobic conditions [1]. They also flourish on synthetic media using various compounds as a single carbon source. Many types of differential and selective media have been developed for the isolation and presumptive testing for *Serratia* species [1]. Media such as nutrient broth, peptone glycerol broth are currently used for the biosynthesis of



prodigiosin [10]. Nakamura [11], used oleic acid substitution instead of sodium oleate and has used only triolein as substrate and reported a yield of 0.69g/ml prodigiosin [11]. The idea of designing a new, nutritious and economically cheap medium was thought of for the prodigiosin biosynthesis. The maximum production of prodigiosin was seen at 28°C and 30 °C in nutrient broth. It did not show pigment production at 37 °C for nutrient broth. Study with an internal adsorbent for prodigiosin in the bioreactor finally yield 13mg/ml [13]. Maltose addition to nutrient broth enhanced pigment production only by 2/4 as at 28 °C and 30 °C. A better source of the substrate in enhancing pigment production in nutrient broth is maltose among the two sugars [1]. Catabolite repression can occur due to addition of glucose or maltose which can cause a reduction in prodigiosin production [13].

## **Methodology and Computational Details**

### **2.3 Density Functional Theory (DFT)**

Density functional theory (DFT) is a modern approach to the solution of many-body quantum mechanical problems in solid state. It is built upon two theorems proposed by Hohenberg and Kohn in 1964. The DFT considers some important terms not considered in earlier computational methods, such as the Hartree-Fock method. DFT, based on Hohenberg- Kohn (HK) theorems [16] and Kohn-Sham (KS) equations [17], is presently the most widely used method to compute the total energy and electronic structure of matter. The DFT uses basic variable including the ground state electron density  $n_0(r)$  of the system, rather than the many electrons wave-functions. DFT further suggests that the electronic density of a system is key to obtaining useful information on its various properties. The huge computational cost associated with the large number of Slater determinants for a many-body system is thus saved in this approach. The two Hohenberg-Kohn theorems described next, show that the spatially

dependent electron density  $n(r)$  is sufficient to determine the ground state energy and properties of the system.

The Density-Functional Theory differs from the wave-function based methods by using the electron density  $n(r)$  as the central quantity. An important advantage of using the electron density over the wave-function is the much-reduced dimensionality. Regardless of how many electrons one has in the system, the density is always three-dimensional. This enables DFT to be readily applied to much larger systems, hundreds or even thousands of atoms become possible. Partly for this reason, DFT has become the most widely used electronic structure approach today, particularly in the condensed matter physics community. The electron density  $n(r)$  is defined as the number of electrons per volume at the point  $r$  in space. It is a physical quantity – it can (at least in theory) be measured. The integral of the electron density gives the total number of electrons:

$$\int n(r)dr = N \quad (2.1)$$

The relation between  $n(r)$  and the many-electron wave-function  $\psi_e$  is:

$$n(r) = N \iint \int |\Psi(r\sigma_1, x_2, \dots, x_N)|^2 d\sigma_1 dx_2 \dots dx_N \quad (2.2)$$

where  $\{x_i\}$  represents both spin and spatial coordinates.  $n(r)$  determines the probability of finding any of the  $N$  electrons with arbitrary spin in a region  $dr$  around  $r$  while the other  $N - 1$  electrons have arbitrary positions and spin in the state represented by  $\psi_e$ .

The electronic energy  $E_e$  can be calculated as the expectation value of the Hamiltonian,

$$E_e = \langle \Psi_e | H_e | \Psi_e \rangle = \langle \Psi_e | T + W + V | \Psi_e \rangle = T + W + V = \iint \dots \int \left( -\frac{1}{2} \sum_{i=1}^N \Psi_e^* \nabla_i^2 \Psi_e + \sum_{i < j}^N \frac{|\Psi_e|^2}{|r_i - r_j|} + \sum_{i=1}^N |\Psi_e|^2 v_{ext}(r_i) \right) d\mathbf{x}_1 d\mathbf{x}_2 \dots d\mathbf{x}_N \quad (2.3)$$

Here  $T$ ,  $W$  and  $V$  are introduced as the individual scalar expectation values of the corresponding operators. If one looks at the three terms in the expression for the

electronic energy Eq. (2.3), one sees that the term for the external potential  $V$  is easily rewritten in terms of the density:

$$\begin{aligned}
 V &= \int \int \cdots \int \sum_{i=1}^N |\Psi_e|^2 v_{\text{ext}}(r_i) \, d\mathbf{x}_1 d\mathbf{x}_2 \cdots d\mathbf{x}_N \\
 &= \frac{1}{N} \sum_{i=1}^N \int n(r_i) v_{\text{ext}}(r_i) \, dr_i = \int n(r) v_{\text{ext}}(r) \, dr
 \end{aligned} \tag{2.4}$$

The other two terms of the electronic energy Eq. (2.3) are not as easy to rewrite. In the kinetic energy term  $T$ , the derivative operator between the wave-functions prevents rewriting the integrand in the form  $[\psi_e]^2$  as needed to turn the term into an expression of the electron density. In the potential energy term  $W$ , the particle positions in the denominator preclude a direct term by term integration.

A functional is an object that acts on a function to produce a scalar. From the way the potential energy term  $V$  was written in Eq. (2.4), it is an explicit potential energy functional  $V[n]$  of the electron density. This and other functionals with the electron density  $n(r)$  as arguments are called density functionals. The other terms in the electronic energy Eq. (2.3) are not in explicit density functional form, but can at least be written as functionals of the many-electron wave-function  $\psi_e^2$ .

$$E_e = T[\Psi_e] + W[\Psi_e] + V[v_{\text{ext}}, n] = F[\Psi_e] + V[v_{\text{ext}}, n] \tag{2.5}$$

The two Hohenberg-Kohn theorems described next, show that the spatially dependent electron density  $n(r)$  is sufficient to determine the ground state energy and properties of the system. And the question of the existence of an  $F[n]$  functional will be considered in the following section.

### 2.3.1 The Thomas-Fermi (TF) Model

Early attempts to express the total internal energy as a density functional was first developed in 1927 by Thomas and Fermi [17]. They used some assumptions about the distribution and interaction between electrons to come close to the kinetic energy while treating the electron-nucleus and electron-electron interactions in a classical manner. The electron density in each space point is set equal to a number of electrons in a fixed volume,  $n(r) = \Delta N / \Delta V$ . A system of  $\Delta N$  free non-interacting electrons in an infinite-well model of volume  $\Delta V$  then gives an expression for the kinetic energy per volume. The continuity limit is then taken  $\Delta V \rightarrow 0$ . The result is integrated over the whole space to give the approximate Thomas-Fermi functional for the total kinetic energy  $T_{TF}[n]$ :

$$T \approx T_{TF}[n] = \frac{3}{10} (3\pi)^{2/3} \int n^{5/3}(r) \, dr \quad (2.6)$$

Furthermore, the electrostatic energy of a classical repulsive gas  $J[n]$  is used as a simplistic approximation of the internal potential energy  $W$ :

$$W \approx J[n] = \frac{1}{2} \iint \frac{n(r)n(r')}{|r-r'|} \, dr \, dr' \quad (2.7)$$

The result is the Thomas-Fermi model:

$$E_e \approx T_{TF} + J[n] + V[v, n] \quad (2.8)$$

The Thomas-Fermi approximation to the internal electronic energy is thus

$$F[n] = T_{TF}[n] + J[n] \quad (2.9)$$

### 2.31 The Hohenberg-Kohn (HK) Theorem

The early efforts to find and use internal electronic energy functionals  $F[n]$  by Thomas and Fermi, and extensions along the same ideas, were all based on 'reasonable' approximations. The work of Hohenberg and Kohn [16] was based on a more rigorous theoretical framework.

Here we examine the two famous theorems which follow from the work of Hohenberg and Kohn:

HK I: The first Hohenberg-Kohn theorem states that the ground state electron density  $n(r)$  determines the external potential of a system  $v_{\text{ext}}(r)$  up to an arbitrary additive constant (which only sets the absolute energy scale).

The proof proceeds by *reductio ad absurdum*. Assume that there exists two local potentials  $v_{\text{ext}}(r)$  and  $v_{\text{ext}}'(r)$  differing by more than an additive constant,  $v_{\text{ext}}(r) \neq v_{\text{ext}}'(r) + \text{const}$ , and giving rise to the same ground-state density,  $n(r)$ . Obviously,  $v_{\text{ext}}(r)$  and  $v_{\text{ext}}'(r)$  belong to distinct Hamiltonians  $\hat{H} = \hat{T} + \hat{W} + \hat{V}$  and  $\hat{H}' = \hat{T} + \hat{W} + \hat{V}'$  which give rise to non-degenerate ground-state wave-functions<sup>1</sup>  $\Psi$  and  $\Psi'$ . Using the Rayleigh-Ritz variational principle, and the fact that  $\Psi$  and  $\Psi'$  have the same density  $n(r)$ , we arrive at the following inequality:

$$\begin{aligned} E_{0'} &< \langle \Psi' | \hat{H} | \Psi' \rangle = \langle \Psi' | \hat{H}' | \Psi' \rangle + \langle \Psi' | \hat{H} - \hat{H}' | \Psi' \rangle \\ &= E_{0'} + \int n(r) [v_{\text{ext}}(r) - v_{\text{ext}}'(r)] dr \end{aligned} \quad (2.10)$$

where  $E_0$  and  $E_{0'}$  are the ground-state energies for  $H$  and  $H'$ , respectively. Similarly, we can get:

$$\begin{aligned} E_{0'} &< \langle \Psi | \hat{H}' | \Psi \rangle = \langle \Psi | \hat{H} | \Psi \rangle + \langle \Psi | \hat{H}' - \hat{H} | \Psi \rangle \\ &= E_0 - \int n(r) [v_{\text{ext}}(r) - v_{\text{ext}}'(r)] dr \end{aligned} \quad (2.11)$$

Adding Eqs. (2.10) and (2.11), we get:

$$E_0 + E_{0'} < E_{0'} + E_0 \quad (2.12)$$

which is clearly a contradiction. We therefore conclude that, for systems without degenerate GS, there cannot exist two local potentials differing by more than an additive constant which

have the same GS density. Thus, the GS density  $n(r)$  determines the potential  $v_{\text{ext}}(r)$ , which in turn determines the Hamiltonian, and thus everything about the many-body problem. In other words, the potential  $v_{\text{ext}}$  is a unique (up to an additive constant) functional of the GS density  $n$ . This means that all GS properties of the system are also consequently determined since in theory anything can be calculated from the external potential. For instance, the GS wave-function  $\psi_0$  is also a GS property of the system and can therefore be considered to be a functional of the GS density  $\psi_0[n]$ . The existence of the total energy functional  $E_e[n]$  and an internal electronic energy functional directly follows as:

$$E_e[n] = \langle \Psi_0[n] | \hat{H}_e | \Psi_0[n] \rangle = \langle \Psi_0[n] | \hat{T} + \hat{W} + \hat{V} | \Psi_0[n] \rangle = F_{\text{HK}}[n] + V[v, n] \quad (2.13)$$

where

$$F_{\text{HK}}[n] = F[\Psi_0[n]] = T[n] + W[n] \quad (2.14)$$

Here note that  $F_{\text{HK}}[n]$  is only dependent on  $n(r)$  and independent of any external potential  $v(r)$ . Thus  $F_{\text{HK}}[n]$  is a universal functional of  $n(r)$ .

HK II: The second Hohenberg-Kohn theorem states that the total energy density functional  $E_e[n]$  satisfies a variational property: the GS energy  $E_0$  of the system considered is obtained by minimizing this functional with respect to  $N$ -electron densities  $n$ .

$$E_0 = \min_n \{ F[n] + \int n(r) v_{\text{ext}}(r) dr \} \quad (2.15)$$

with the minimum being reached for the exact GS density  $n_0(r)$ . We can express this as  $E_0[n_0] \leq E_e[n]$ .

The proof follows straightforwardly from the first theorem. Suppose  $\psi$  is the GS wave-function corresponding to the unique GS density  $n_0(r)$ , we then define the energy of the GS by:

$$E_0 = E_e[n_0] = \langle \Psi | \hat{H}_e | \Psi \rangle \quad (2.16)$$

If there is another wave-function  $\psi'$  with an arbitrary variation from  $\psi$  and its

electron density is  $n_0(r)$ , then we can obtain

$$E_0 = E_e[n_0] = \langle \Psi | \hat{H}_e | \Psi \rangle < \langle \Psi' | \hat{H}_e | \Psi' \rangle = E_e[n'] \quad (2.17)$$

So, it follows that the correct density that minimizes the energy is the GS density. The many-electron problem has thus been rewritten into what looks like a straightforward minimization with respect to a three-dimensional quantity  $n(r)$ . Yet the functional form of  $F_{\text{HK}}[n]$  is not known and this poses a serious challenge for practical applications. The major part of the complexities of the many-electron problem are associated with the determination of the universal functional  $F_{\text{HK}}[n]$ .

## 2.32 Wave-Function Based Methods

As mentioned earlier, the fundamental quantity for the wave-function based methods is the many-electron wave-function,  $\psi_e$ , whose correct functional form is far from simple. The first step in the determination of  $\psi_e$  is often simply an ansatz (an educated guess) and then reliance on the variational principle. The variational principle says that we can use any normalized wave-function to calculate the expectation value of the electronic Hamiltonian ( $H_e$ ) and we are guaranteed to get an energy above the true ground-state (GS) energy i.e.,  $E[\psi_e] \geq E_0[\psi_0]$ . The equality holds only when the wave-function  $\psi_e$  is in the true GS ( $\psi_0$ ). The advantage of the variational principle is that starting with a trial wave-function we can approach the GS energy  $E_0[\psi_0]$  from above by variationally improving the quality of the wave-function. In the following, the variational principle will be applied to minimize the energy and obtain the Hartree-Fock equation and wave-function.

### 2.3.3 Exchange-correlation functional

The exchange-correlation term ( $E_{\text{xc}}$ ) is the energy contribution from the quantum effects not included in the Coulomb repulsion and the single-particle kinetic energy. The exact form of

$E_{xc}$  is not known and may never be known (in a closed mathematical form). Thus, since the birth of DFT some sort of approximations for  $E_{xc}$  have been used. We review here the main classes of approximate xc functionals. These classes are roughly ordered from the simplest to the most sophisticated ones as proposed by Perdew [18] and is known as “Jacob’s ladder”. In this scheme, functionals are grouped according to their complexity on rungs of a ladder which lead from the Hartree approximation on “earth” to the exact xc functional in “heaven”. The first few rungs of this ladder are now briefly discussed as a means to introduce some of the most common types of xc functionals in widespread use. The discussion is focus on the contents of the approximations, not their performance in practical calculations. On the average, more sophisticated approximations are usually more accurate than simpler ones, even though many exceptions can be found. The commonly used approximations to determine the exchange-correlation energy include the local density approximation (LDA), generalized gradient approximation (GGA), and hybrid functionals. These approximations are discussed below.

### 2.3.4 The Local-Density Approximation (LDA)

In the local-density approximation (LDA), introduced by Kohn and Sham [17], the xc functional is approximated as:

$$E_{xc}^{LDA}[n] = \int n(r) \epsilon_{xc}^{unif}(n(r)) dr \quad (2.18)$$

where  $\epsilon_{xc}^{unif}$  is the exchange-correlation energy per particle of the interacting uniform electron gas with the density  $n(r)$ ? The uniform electron gas represents a family of systems of interacting electrons with an arbitrary spatially constant density  $n(r)$  that acts as a parameter. Thus, in the LDA, the exchange-correlation energy per particle of an inhomogeneous system at a spatial point of density  $n(r)$  is approximated as the exchange-correlation energy per



particle of the uniform electron gas of the same density. The function  $\epsilon_{xc}^{unif}(n)$  is a sum of exchange and correlation contributions,  $\epsilon_{xc}^{unif}(n) = \epsilon_x^{unif}(n) + \epsilon_c^{unif}(n)$ . The exchange energy per particle of the uniform electron gas can be calculated analytically

$$\epsilon_x^{unif}(n) = c_x n^{1/3} \quad (2.19)$$

Where  $c_x = -(3/4)(3/\pi)^{1/3}$

Thus, we have the exact analytical expression for the exchange energy:

$$E_x^{LDA}[n] = -\frac{3}{4} \left(\frac{3}{\pi}\right)^{1/3} \int n^{4/3}(r) dr \quad (2.20)$$

The correlation energy per particle  $\epsilon_c^{unif}(n)$  of the uniform electron gas cannot be calculated analytically. This quantity has been obtained numerically for a number of densities  $n$  using accurate quantum Monte Carlo simulations of the UEG [18], and fitted to a parametrized function of  $n$  satisfying the known high- and low-density expansions. Expressed in terms of the Wigner-Seitz radius  $r_s$ , the first terms of the high-density expansion ( $r_s \rightarrow 0$ ) have the form

$$\epsilon_c^{unif} = A \ln r_s + B + C r_s \ln r_s + \mathcal{O}(r_s), \quad (2.21)$$

and the first terms of the low-density expansion ( $r_s \rightarrow +\infty$ ) have the form

$$\epsilon_c^{unif} = \frac{a}{r_s} + \frac{b}{r_s^{3/2}} + \mathcal{O}\left(\frac{1}{r_s^2}\right), \quad (2.22)$$

where  $A$ ,  $B$ ,  $C$ ,  $a$ , and  $b$  are constants depending on the electron spin configuration. The Perdew-Zunger [19], Perdew-Wang (PW) [20] and Vosko-Wilk-Nusair (VWN) functionals are all common LDA functionals.

### 2.3.5 The Generalized-Gradient Approximation (GGA)

It was realized very early that only the local uniform density at each given point is not a reasonable approximation for the rapidly varying electron densities of many materials, and

that the gradient of the density ( $\nabla n(r)$ ) needs to be included. A first attempt was the so-called gradient-expansion approximations (GEA). The idea behind GEA is to regard LDA as the first term in a power series expansion of  $E_{xc}$  in the density's spatial variation (described by the derivatives of  $n(r)$ ). The second-order GEA thus uses LDA plus the term of next lowest order in density variation, giving a functional of the form

$$E_{xc}^{GEA}[n] = E_{xc}^{LDA}[n] + \int A_{xc}(n(r))s^2 + \int B_{xc}(n(r))q + \dots \quad (2.23)$$

where  $A_{xc}(n(r))$  and  $B_{xc}(n(r))$  are dimensionless functions (not functionals) of  $n(r)$ , and  $s$  and  $q$  define the appropriate measure of the density gradient both of which have been expressed on scale invariant form; the dimensionless gradient

$$s = \frac{|\nabla n|}{2k_F n} = \frac{|\nabla n(r)|}{2(3\pi^2)^{1/3} n^{4/3}(r)} = \frac{3}{2} \left( \frac{4}{9\pi} \right)^{1/3} |\nabla r_s| \quad (2.24)$$

and the dimensionless Laplacian

$$q = \frac{\nabla^2 n}{(2k_F)^2 n} = \frac{\nabla^2 n(r)}{4(3\pi^2)^{2/3} n^{5/3}(r)} \quad (2.25)$$

Because there is no special direction in the uniform electron gas, there can be no term linear in  $\nabla n$ . Moreover, terms linear in  $\nabla^2 n$  can be recast as  $s^2$  terms via integration by parts, since:

$$\int dr f(n) \nabla^2 n = - \int dr \left( \frac{\partial f}{\partial n} \right) |\nabla n|^2 \quad (2.26)$$

In application to real systems, the GEA has generally been disappointing, indeed often worsened the results of the LDA. The failure of the GEA lead to the development of generalized-gradient approximation (GGA). The xc functional is written as a function of the local density and of the local gradient of the density, usually as an "enhancement factor"  $F_{xc}$  multiplying the homogeneous electron:

$$E_{xc}^{GGA}[n] = \int \varepsilon_{xc}(n(r)) F_{xc}(n(r), \nabla n(r)) dr \quad (2.27)$$

The enhancement factor is written in terms of  $r_s$  and the dimensionless density gradient  $s$ :

$$F_{xc}(n(r), |\nabla n(r)|) \rightarrow F_{xc}(r_s, s)$$

Gradient-corrected functionals are the simplest extensions of LDA to inhomogeneous systems one can think of. GGA found widespread acceptance due to their improved performance. GGA functionals are known to satisfy some known conditions that the exact functional should satisfy as well [21]. They yield much better atomic energies and binding energies than LDA, at a modest additional computational cost [22]. In particular, they yield better results for the band gap in semiconductors and insulators especially for some transition-metal oxides which LDA incorrectly describes as metals [23]. Despite the improvement by GGA over LDA functions, even greater accuracy can be obtained by using the so-called meta-GGA.

### 2.3.6 Meta-GGA (mGGA)

The next step in the development of gradient approximations is to incorporate the kinetic energy density or/and the Laplacian of the density. Such functionals are generally referred to as meta-GGA functionals.

The form of the functional is typically:

$$E_{xc}^{mGGA} = \int n(r) \varepsilon_{xc}(n, |\nabla n|, \nabla^2 n, \tau) dr \quad (2.28)$$

where the kinetic energy density  $\tau$  is;

$$\tau = \frac{1}{2} \sum_i |\nabla \phi_i|^2 \quad (2.29)$$

Still higher accuracy (of course, at a higher cost) can be obtained by using the so-called hybrid schemes.

### 2.3.7 Hybrid Schemes

These fourth generation functionals add “exact exchange” calculated from the HF-like functional to some conventional treatment of DFT exchange and correlation:

$$E_{xc}^{\text{hybrid}} = \alpha E_x^{\text{HF}} + E_c \quad (2.30)$$

where  $\alpha$  can be chosen to satisfy particular criteria. The B3LYP functional [24], which is widely used in the quantum chemistry community [25], is an example. Here three adjustable parameters ( $a_1 - 3$ ) are used to fit calculated values to a molecular data base. It has the following form:

$$E_{xc} = E_{xc}^{\text{LDA}} + a_1(E_x^{\text{HF}} - E_x^{\text{LDA}}) + a_2\Delta E_x^{\text{GGA}} + a_3\Delta E_c^{\text{GGA}} \quad (2.31)$$

Where  $E_{xc}^{\text{LDA}}$  and  $E_x^{\text{HF}}$  and  $E_x^{\text{LDA}}$  are the LDA exchange-correlation energy functional, Hartree-Fock exchange energy functional and LDA exchange energy functional respectively.

$\Delta E_x^{\text{GGA}}$  and  $\Delta E_c^{\text{GGA}}$  are respectively the gradient-corrected exchange and correlation functionals. As mentioned earlier, the functionals currently used in density functional simulations form a natural hierarchy. Although, it cannot be claimed that there is a systematic approach to the exact functional, it is clear that improvements are being made in the underlying functional form and that the description of ground state properties is improving. The most notable recent advances being those in which the non-local nature of the exchange potential is introduced in one form or another.

#### 2.3.1 Basis Sets

Basis sets are almost always necessary for the practical solution of Kohn-Sham equations. Essentially, almost all electronic structure methods today rely on an expansion of the unknown wave function in terms of a set of basis functions. Any type of basis function may in principle be used like exponential, Gaussian, polynomial, planewave, spline, Slater type

orbitals, and numeric atomic orbitals, and so forth. In this thesis, the calculations we do for periodic systems are carried out with plane wave basis sets and pseudo-potentials. Also, the approach of combining plane wave basis sets and pseudo-potentials is the workhorse of the present day DFT calculations for periodic systems, so we briefly discuss such methods.

### 2.3.2 Plane Waves

For the treatment of periodic systems, like solids, plane wave basis sets have become the natural choice because of Bloch's theorem. In a periodic potential,  $U(\mathbf{r})$ , where  $U(\mathbf{r} + \mathbf{R}) = U(\mathbf{r})$  and  $\mathbf{R}$  is the Bravais lattice vector, Bloch's theorem states that the eigenfunctions of the one-electron Hamiltonian  $H = -\frac{1}{2}\nabla^2 + U(\mathbf{r})$  can be chosen to have the form of a plane wave ( $e^{i\mathbf{k}\cdot\mathbf{r}}$ ) times a function,  $u_{nk}(\mathbf{r})$ , having the same periodicity as the potential  $U(\mathbf{r})$ :

$$\phi_{nk}(\mathbf{r}) = e^{i\mathbf{k}\cdot\mathbf{r}} u_{nk}(\mathbf{r}) \quad (2.32)$$

where  $u_{nk}(\mathbf{r} + \mathbf{R}) = u_{nk}(\mathbf{r})$ . Here the index  $k$  reflects the periodicity of the system, the index  $n$  is a second quantum number, the so-called "band index", and it originates from the atomic states which form the Bloch states  $\phi_{nk}$ : for any value of  $k$  one finds a complete set of bands  $n$ .

Bloch's theorem allows to expand the electronic wave function in terms of a discrete set of plane waves. But, for a periodic solid which has electrons in the order of Avogadro's number, the spacing of the  $\mathbf{k}$  points goes to zero and  $\mathbf{k}$  can be considered as a continuous variable. So far the infinite number of electrons in the solid are accounted for by an infinite number of  $\mathbf{k}$  points, and only a finite number of electronic states are occupied at each  $\mathbf{k}$  point. The occupied states at each  $\mathbf{k}$  point contribute to physical quantities such as the electronic potential, electron density, and total energy of the solid. However, the electronic wave

functions at  $\mathbf{k}$  points that are very close together will be almost identical. Hence it is possible to represent them over a region of  $\mathbf{k}$  space only by that single  $\mathbf{k}$  point. Efficient methods have been devised to choose special finite sets of  $\mathbf{k}$  points, for obtaining an accurate electronic potential, electron density, and total energy. In this thesis, the method proposed by Monkhorst and Pack [60] has been used, in which a uniform mesh of  $\mathbf{k}$  points is generated along the three lattice vectors in reciprocal space. The magnitude of any error in the total energy or the total energy difference due to inadequacy of the  $\mathbf{k}$  point sampling can always be reduced to zero by using a denser set of  $\mathbf{k}$  points. Therefore, it is crucial to test the convergence of the results with respect to the number of  $\mathbf{k}$  points in general.

Now expanding the periodic function  $u_{nk}$  with plane waves whose wave vectors are reciprocal lattice vectors ( $\mathbf{G}$ ) of the periodic crystal:

$$u_{nk}(r) = \sum_{\mathbf{G}} C_{n,\mathbf{G}} e^{i\mathbf{G}\cdot r} \quad (2.33)$$

so the electronic wave function can be rewritten as:

$$\phi_{nk}(r) = \sum_{\mathbf{G}} C_{n,\mathbf{k}+\mathbf{G}} e^{i(\mathbf{k}+\mathbf{G})\cdot r} \quad (2.34)$$

While solving one electron Schrödinger-like equation with an effective periodic potential, e.g., the Kohn-Sham potential defined in Eq. (53), the Kohn-Sham wave function can be expanded with plane wave basis sets as described in Eq. (108). As a result Eq. (55) can be rewritten as:

$$\sum_{\mathbf{G}'} \left[ \frac{1}{2} |\mathbf{k} + \mathbf{G}'|^2 \delta_{\mathbf{G},\mathbf{G}'} + V_{\text{eff}}(\mathbf{G} - \mathbf{G}') \right] C_{n,\mathbf{k}+\mathbf{G}'} = \epsilon_n C_{n,\mathbf{k}+\mathbf{G}} \quad (2.35)$$

where  $\delta_{\mathbf{G},\mathbf{G}'}$  is the Kronecker  $\delta$  and reflects that the kinetic energy is diagonal and  $\epsilon_n$  are the electronic energies. The above equation is the basic Schrödinger-like equations of a periodic crystal with a plane wave basis set.

Here the sum over  $\mathbf{G}'$  tells that one needs an infinite number of plane waves to solve Eq.(2.35). However, the coefficients  $C_{n,\mathbf{k}+\mathbf{G}}$  for the plane waves with small kinetic energy are typically more important than those with large kinetic energy. Thus, the plane wave basis set can be truncated to include only plane waves that have kinetic energies less than a particular energy cutoff  $E_{\text{cut}}$ :

$$\frac{1}{2}|\mathbf{k} + \mathbf{G}|^2 \leq E_{\text{cut}} \quad (2.36)$$

Employing a finite basis set introduces a new source of inaccuracy, which can be reduced by increasing the number of plane waves or  $E_{\text{cut}}$ . Therefore, appropriate convergence tests have to be performed in order to find an  $E_{\text{cut}}$  that is sufficiently converged to compute the property of interest with the required accuracy.

## 2.4 Frontier Molecular Orbitals

The frontier molecular orbitals can offer a reasonable qualitative prediction of the excitation properties and the ability of electron transport [26]. The energies of HOMO and LUMO are negative, which indicates that the studied compound is stable [27]. The molecular orbital (MO) is a very important concept in quantum chemistry being extensively employed to describe the chemical behaviour [28]. The highest occupied molecular orbital (HOMO) and lower unoccupied molecular orbital (LUMO) are the two most important molecular orbitals in a molecule as both are used to describe various chemical properties such as reactivity and kinetics [29]. Also, these orbitals are an indispensable tool for the description of other phenomena involving molecular electronic structures, such as charge transfer, photoexcitation, and molecular electronics [30]. Using HOMO and LUMO orbital energies, the

ionization energy and electron affinity can be expressed as:  $I = -E_{\text{HOMO}}$ ,  $A = -E_{\text{LUMO}}$ ,  $\eta = (-E_{\text{HOMO}} + E_{\text{LUMO}})/2$  and  $\mu = (E_{\text{HOMO}} + E_{\text{LUMO}})/2$  [31].

The highest occupied molecular orbitals (HOMOs) and the lowest lying unoccupied molecular orbitals (LUMOs) are named as frontier molecular orbitals (FMOs). The FMOs play an important role in the optical and electric properties, as well as in quantum chemistry and UV-Visible spectra [32]. The HOMO represents the ability to donate an electron and LUMO represents electron acceptor tendency. The energy gap between HOMO and LUMO reflects the chemical reactivity, polarizability and chemical hardness/softness of a molecule [33]. The hard molecules are difficult to polarize than the soft ones as they need high energy for excitation. The HOMO-LUMO energy separation has served as a simple measure of kinetic stability [34]. A molecule with a small or no HOMO-LUMO gap is chemically reactive [34].

#### **2.4.1 HOMO-LUMO**

Many organic molecules, containing conjugated p electrons are characterized by large values of molecular first hyperpolarizabilities, were analysed by means by vibrational spectroscopy. The interaction of two atomic (or) molecule orbital produces two new orbitals. One of the new orbitals is higher in energy than the original ones (the anti-bonding orbital) and one is lower (the lower orbital) [35]. Highest occupied molecular orbital (HOMO) and lowest unoccupied molecular orbital (LUMO) are frontier molecular orbitals that play important role in predicting chemical reactivity as well charge transfer properties of the molecule [36]. HOMO, LUMO energy characterizes the ability of electron accepting. When one of the initial orbitals is filled with a pair of electrons (a Lewis base) and the other is empty (a Lewis acid), we can place the two electrons into the lower, energy of the two new orbitals. The "Filled-Empty" interaction therefore is stabilizing. When we are dealing with interacting molecular



orbitals, the two that interact are generally the highest energy occupied molecular orbital (HOMO) and lowest unoccupied molecular orbital (LUMO) of the compound [37]. These orbitals are a pair of orbitals in the compound, which allows them to interact most strongly. These orbitals are sometimes called the frontier orbitals, because they lie at the outermost boundaries of the electrons of compound. The HOMO-LUMO energy gap reveals that the energy gap reflects the chemical activity of the molecule. LUMO as an electron acceptor represents the ability to obtain an electron, HOMO represents the ability to donate an electron. Moreover, the lower value in the HOMO and LUMO energy gap explains the eventual charge transfer interactions taking place within the molecule [35]. In terms of chemical hardness, a large HOMO-LUMO gap indicates a hard molecule and is related to more stable molecules, whereas a small gap indicates a soft molecule and is related to a more reactive molecule [38].

## **2.5 Electrostatic Potential**

Molecular Electrostatic Potential (MEP) is defined as the electrostatic (Coulomb) potential created in the neighbouring space by the nuclear charges and the electronic distribution of a molecule [39]. Electrostatic potential maps, also known as electrostatic potential energy maps, or molecular electrical potential surfaces, illustrate the charge distributions of molecules three dimensionally [40]. These maps allow us to visualize variably charged regions of a molecule. Knowledge of the charge distributions can be used to determine how molecules interact with one another [41]. Electrostatic potential maps are very useful three-dimensional diagrams of molecules. They enable us to visualize the charge distributions of molecules and charge related properties of molecules [42]. They also allow us to visualize the size and shape of molecules [43]. In organic chemistry, electrostatic potential maps are invaluable in predicting the behaviour of complex molecules. The molecular electrostatic

potential (MEP) maps have been used to predict the behaviour and reactivity of the molecules. It is mapping potentials created in the space around a molecule by its nuclei and electrons [27]. MEP map is very useful for the qualitative interpretation of the electrophilic and nucleophilic reactions for the study of biological recognition process and hydrogen bonding interactions [44]. This also provides information for understanding the shape, size, charge density, delocalization and site of chemical reactivity of the molecules. MEP can be measured experimentally by diffraction as well as it can be computed by quantum mechanical methods [38]. MEP maps can be obtained by mapping electrostatic potential onto the total electron density with colour code [45]. There are three important colours; blue, red and green used to indicate the value of the electrostatic potential. The surfaces with blue and red colours show the positive and negative values of the potential respectively. The surfaces with green colours indicate zero potential [36].

The concept of the electrostatic potential as a quantum mechanical observable (the expectation value of the one-electron operator  $r^{-1}$ ) probing the molecular charge distribution and its usage as a tool for describing molecular interactions and chemical reactivity is well documented [46]. The development of procedures to generate classical partial atomic charges from the quantum mechanical electrostatic potential provides well-defined methods for obtaining electrostatic interaction parameters required in molecular mechanics and dynamics simulation [47].

## **2.6 Solvent Accessibility Surface Area**

solvent-accessible surface area (SASA) is the surface area of a biomolecule that is accessible to a solvent. Measurement of ASA is usually described in units of square Angstroms. The concept of the solvent accessible surface of a protein molecule was originally introduced in

1971, as a way of quantifying hydrophobic burial [48]. In macromolecules, such as peptides  
Assessible surface areas is a measure of thermodynamic parameters [49].

Molecules are often represented as a set of overlapping spheres [48]. The solvent-accessible surface area (SASA) of a molecule is widely used in describing solvation of solutes and macromolecules [50]. The SASA is defined as the surface traced by the centre of a sphere rolled over the van der Waals surface [48]. The free energy of aqueous solvation, at least for nonpolar molecules, is linearly related to SASA. Therefore, many methods some exact, some approximate— have been presented to calculate analytical atomic SASAs and their partial derivatives with respect to atomic coordinates [51].

For evaluation of this volume, the radii of the balls should be put to the van der Waals radii of the corresponding atoms augmented by the effective radius of the water molecule ( $1.4 \text{ \AA}$ ) [48]. The second term accounts for the energy of the van der Waals interactions and the hydrophobic/hydrophilic effects. The contribution to this term from each atom is proportional to the area of its surface that is exposed to the solvent (also called the solvent accessible surface area, SASA). More precisely, this area can be defined as the uncovered surface area of the corresponding ball, with the ball radii being specified above [52].

## CHAPTER THREE

### COMPUTATIONAL DETAILS

This section shall discuss the computations details and approached employed in modelling the Prodigiosin molecule. The initial structure of the prodigiosin molecule was constructed using the ArgusLab Software version 4.0.1. The generated was subjected to geometry optimisation using the VASP - Vienna Ab initio Simulation Package [53] [54] [55], which performs DFT calculations. The projected augmented wave (PAW) method was used to describe the interactions between the valence and cores electrons [56] [57]. The electronic exchange–correlation potential was calculated using the Perdew–Burke–Ernzerhof (PBE) generalized gradient approximation (GGA) functional [58] [59]. Long-range vdW interactions were accounted for using the Grimme DFT-D3 scheme [60]. A plane-wave basis set with a kinetic energy cut-off of 600 eV was tested to be sufficient to converge the total energy of the Prodigiosin molecule to within  $10^{-6}$  eV and the residual Hellmann–Feynman forces on all relaxed atoms reached  $10^{-3}$  eV Å<sup>-1</sup>. A Monkhorst–Pack k-points mesh of 1×1×1 was used to sample Brillouin zone, which ensures electronic and ionic convergence. The optimized geometry from DFT calculations were imported into the ArgusLab software for the generation and analyses of the HOMO-LUMO iso-contours, electrostatic potential map and solvent accessibility surface area. Viewing and adjusting the molecular structure, atomic sizes, atomic distances, lattices parameters, and arrangement of the atoms was done with the aid of VESTA, Avogadro and Xcrysden packages.

## CHAPTER FOUR

### RESULTS AND DISCUSSION

#### 4.1 Optimized Molecular Structure of Prodigiosin and Geometry Parameters

The optimized geometry structure of the prodigiosin molecule is shown in Figure 4.1. The interatomic bond distances and angles relative to the reference numbers shown in Figure 4.1 are listed in Table 4.1 and Table 4.2, respectively. The C-C bond lengths from table 4.1 ranges from 1.3817 Å – 1.540 Å. The highest bond length is between C12-C13 and the shortest bond length is between C17-C20. C-O bond lengths represented by O49-C5 with bond length 1.3515 Å and O49-C5 with bond length 1.4332 Å.

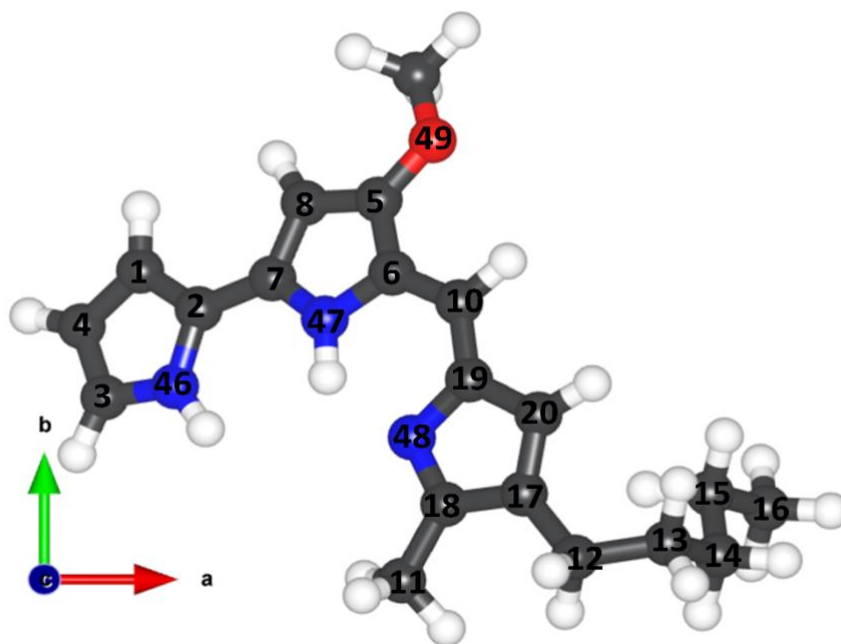


**FIGURE 4. 1: OPTIMIZED GEOMETRY OF PRODIGIOSIN MOLECULE. COLOUR CODE: CARBON = RED, OXYGEN = RED, NITROGEN = BLUE, HYDROGEN = WHITE.**

The C-N bond lengths are N48-C18 (1.3322 Å), N48-C19 (1.4064 Å), N47-C6 (1.3891 Å), N47-C7 (1.3612 Å), N46-C3 (1.3754 Å), and N48-C2 (1.3855 Å). The highest C-N bond length being

N48-C2 (1.3855 Å) and the lowest which is N48-C19 (1.4064 Å). The difference in the bond lengths is as a result of the influence of the pyrrole group. The bond angles for C-N-C are C3-N46-C2 (169.926 degrees), C7-N47-C6 (110.561 degrees) and C19-N48-C18 (105.813 degrees). The lowest shows the highest delocalization.

**TABLE 4. 1: GEOMETRY OPTIMIZED INTERATOMIC BOND DISTANCES IN PRODIGIOSIN**

ATOM	DISTANCE (Å)	ATOM	DISTANCE (Å)
C4-C3	1.3876	C18-C11	1.4942
C1-C4	1.4126	C17-C12	1.5002
C1-C2	1.3978	C12-C13	1.54
C2-C7	1.4342	C13-C14	1.5386
C7-C8	1.4139	C14-C15	1.533
C8-C5	1.3996	C15-C16	1.5318
C5-C6	1.4265	N48-C18	1.3322
C6-C10	1.4041	N48-C19	1.4064
C10-C19	1.3907	N47-C6	1.3891
C19-C20	1.442	N47-C7	1.3612
C20-C17	1.3817	N46-C3	1.3754
C17-C18	1.4565	N46-C2	1.3855

**TABLE 4. 2: GEOMETRY OPTIMIZED BOND ANGLES IN PRODIGIOSIN**

ATOMS	ANGLE (DEGREE)
C3-N46-C2	109.926
C7-N47-C6	110.561
C5-O49-C9	115.667
C19-N48-C18	105.813
C4-C1-C2	108.003
C1-C4-C3	107.433
C5-C8-C7	106.824
C6-C10-C19	124.817
C19-C20-C17	106.953
C20-C17-C19	129.656
C17-C18-C11	125.732
C17-C12-C13	117.657
C12-C13-C14	116.229
C13-C14-C15	116.394
C14-C15-C16	112.534
C8-C7-C2	126.868
C7-C2-C1	128.611
C5-C6-C10	131.605
C2-C7-N47	125.314

## 4.2 Mulliken Atomic Charges

The calculated Mulliken [61] charges, which helps ascertain the electron population of each atom in the prodigiosin molecule are summarized in Table 4.3. The Mulliken charges on hydrogen atoms are seen to be positive. Oxygen and nitrogen atoms show negative charges. Some carbon atoms C2, C3, C5, C6, C7, C9, C17, C18 and C19 have positive charges whereas the rest are negative, indicating the direction of delocalization.

**TABLE 4. 3: MULLIKEN ATOMIC CHARGES OF PRODIGIOSIN**

Element	Charge	Element	Charge	Element	Charge	Element	Charge
1 C	-0.0825	16 C	-0.155	31 H	0.0762	46 H	0.0477
2 C	0.0669	17 C	0.0183	32 H	0.0663	47 H	0.0498
3 C	0.0543	18 C	0.2306	33 H	0.0748	48 H	0.0492
4 C	-0.1121	19 C	0.1263	34 H	0.0448	49 H	0.0698
5 C	0.1857	20 C	-0.1179	35 H	0.0596		
6 C	0.1543	21 N	-0.3521	36 H	0.0688		
7 C	0.1993	22 N	-0.3899	37 H	0.0545		
8 C	-0.1139	23 N	-0.558	38 H	0.0535		
9 C	0.0025	24 O	-0.3847	39 H	0.0491		
10 C	-0.138	25 H	0.0669	40 H	0.0397		
11 C	-0.1349	26 H	0.0967	41 H	0.0526		
12 C	-0.0859	27 H	0.0697	42 H	0.0443		
13 C	-0.0944	28 H	0.2394	43 H	0.047		
14 C	-0.0926	29 H	0.2621	44 H	0.0485		
15 C	-0.0934	30 H	0.078	45 H	0.058		



### 4.3 Frontier Molecular Orbital: HOMO and LUMO

The frontier molecular orbitals can offer a reasonable qualitative prediction of the excitation properties and the ability of electron transport in the molecule as shown by [62]. The energies of HOMO and LUMO are negative, which indicates that the studied compound is stable [63]. Using HOMO and LUMO orbital energies, the ionization energy and electron affinity can be expressed as:  $I = -E_{\text{HOMO}}$ ,  $A = -E_{\text{LUMO}}$ ,  $\eta = (-E_{\text{HOMO}} + E_{\text{LUMO}})/2$  and  $\mu = (E_{\text{HOMO}} + E_{\text{LUMO}})/2$  [31]. Parr et al., [64] proposed the global electrophilicity power of a ligand as  $\omega = \mu^2/2\eta$ . The hardness  $\eta$  and chemical potential  $\mu$  are given by the following relations:  $\eta = (I - A)/2$  and  $\mu = -(I + A)/2$ , where  $I$  and  $A$  are the first ionization potential and electron affinity of the chemical species [27]. For the title compound,  $E_{\text{HOMO}} = -3.687$  eV,  $E_{\text{LUMO}} = -2.254$  eV, Energy gap =  $E_{\text{LUMO}} - E_{\text{HOMO}} = 1.433$  eV, Ionization potential  $I = 3.687$  eV, Electron affinity  $A = 2.254$  eV, global hardness  $\eta = 0.7165$  eV, chemical potential  $\mu = -2.9705$  eV and global electrophilicity =  $\mu^2/2\eta = 6.1576$  eV. The energy gap between HOMO and LUMO reflects the chemical reactivity, polarizability and chemical hardness/softness of a molecule. This lower gap allows it to be the softest molecule. Kinetic stability decreases with the decrease of HOMO-LUMO gap. As a result, removal of electrons from ground state HOMO to excited state LUMO requires less energy. The diagrammatic representation of the HOMO and LUMO for the optimized prodigiosin molecule is shown in Figures 4.2 and figure 4.3, respectively.

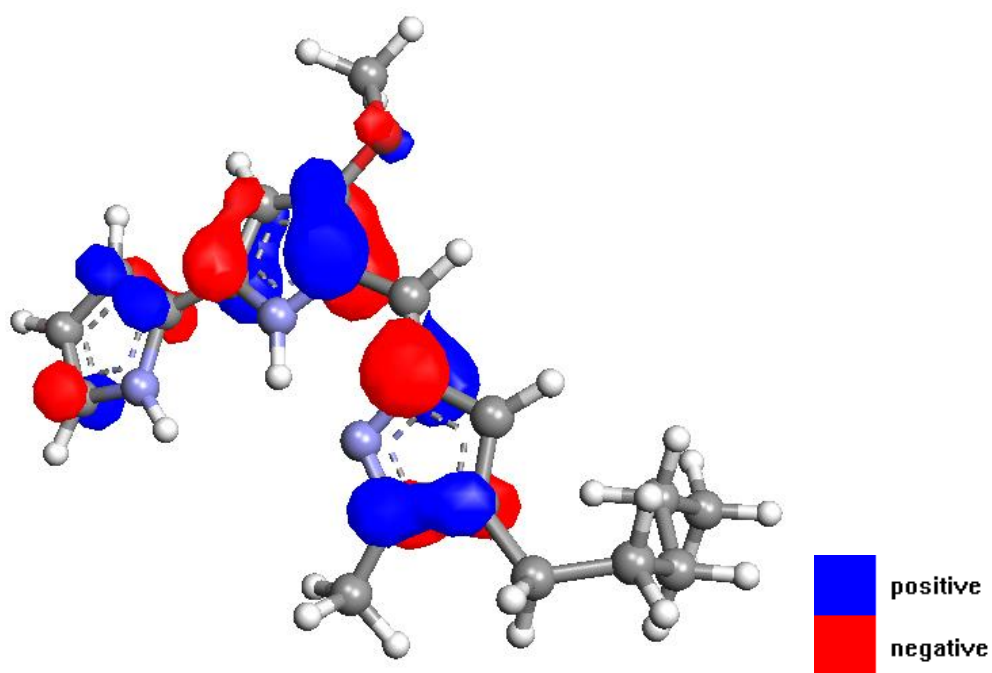


FIGURE 4. 2: HIGHEST OCCUPIED MOLECULAR ORBITAL DIAGRAM OF PRODIGIOSIN

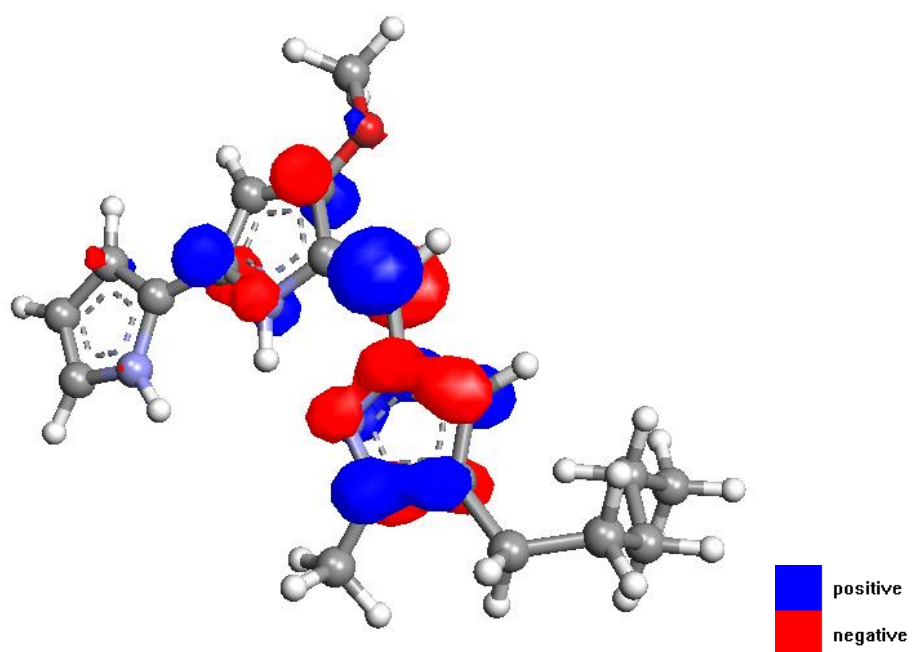


FIGURE 4. 3: LOWEST UNOCCUPIED MOLECULAR ORBITAL DIAGRAM OF PRODIGIOSIN

#### 4.4 Electrostatic Potential Map (ESP)

Electrostatic potential map is an important descriptor used in understanding sites for both nucleophilic and electrophilic reactions [65] as well as for the study of biological recognition process [40]. Figure 4.5 provides a visual presentation of the chemically active sites and comparative reactivity of atoms. Potential value increases in the order red < orange < yellow < green < blue. The negative (red and yellow) regions of ESP are related to electrophilic reactivity and the positive (blue) regions to nucleophilic reactivity. From the ESP map of the Mapped surface was generated using ArgusLab software. This is a surface where one property is superimposed onto a surface created by another property. A negative ESP, is often a vicinity of stability for test charge. On the other hand, a positive ESP, is often a vicinity of relative instability for the positive test charge. The sites of the molecule which are susceptible to nucleophilic or electrophilic attack can be seen using ESP-mapped density surface as shown in figure 4.5. This surface is helpful for qualitative interpretations of chemical reactivity. Here, the maximum negative potentiality to be -0.500 a.u (deepest red) for oxygen atom and the highest positive potentiality of +0.0136 a.u (deepest blue) of other atoms.

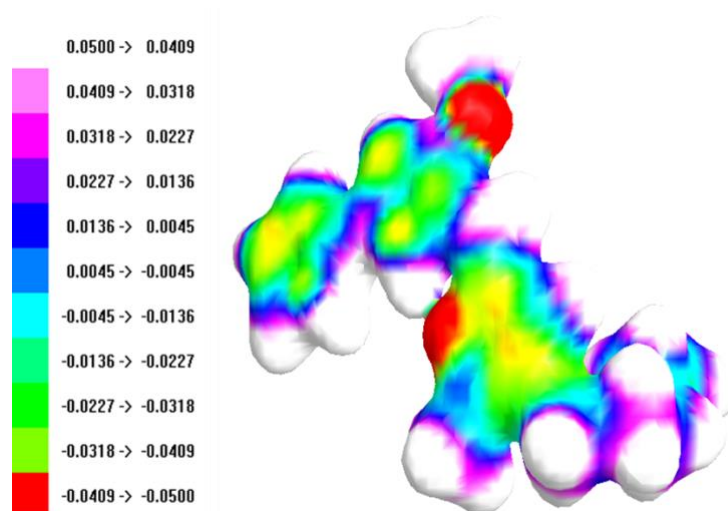


FIGURE 4. 4: ELECTROSTATIC POTENTIAL-MAPPED ELECTRON DENSITY SURFACE OF PRODIGIOSIN

## 4.5 Solvent Accessibility Surface Area

The solvent accessibility of the prodigiosin molecule is shown in Figure which shows the highest value of 103 square Å. This is a large surface area for interaction and accessibility to water medium when used as a cancer drug as it will find itself in an aqueous media.

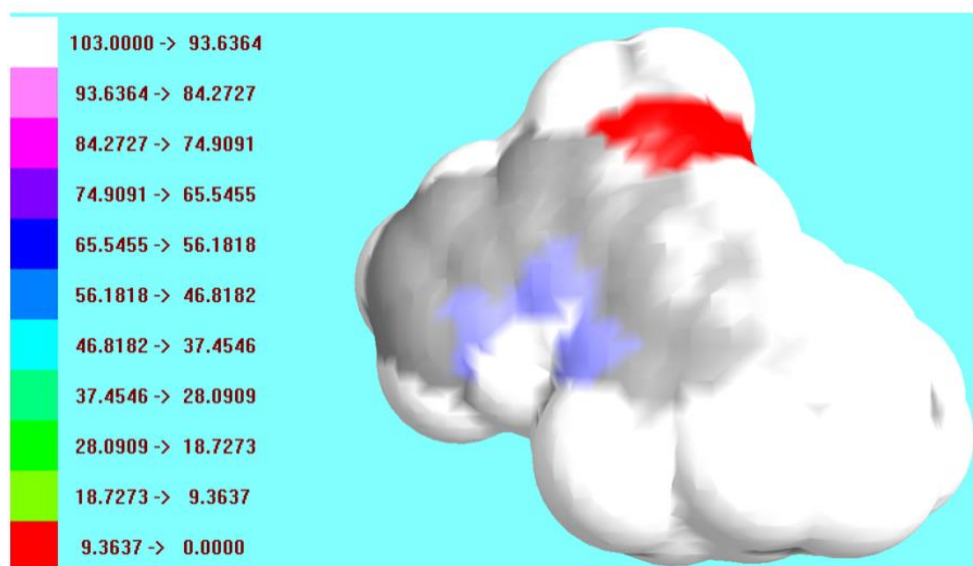


FIGURE 4. 5: SOLVENT ACCESSIBILITY SURFACE AREA OF PRODIGIOSIN

## CHAPTER FIVE

### SUMMARY AND CONCLUSIONS

In the work, the structural and electronic properties of the prodigiosin, a potential cancer drug was comprehensively characterized using computational approaches based on density functional theory calculations. Geometric parameters including interatomic bond distances and angles are systematically characterized. The Electrostatic potential map (ESP) map of the prodigiosin molecule shows that the negative potential sites are around O49 (oxygen) and N48 (one of the nitrogen atom) and the positive potential site are around the carbon atoms. The sites provide information about the possible reaction regions of the prodigiosin molecule. The value of the energy separation between HOMO and LUMO is very small compared to other compounds and this energy gap gives valuable information about the reactivity of the molecule. As ESP predicts the most reactive part of the molecule, the chemical reactivity is also understood from its chemical potential, electrophilicity and hardness. The solvent accessibility surface area of the molecule better understanding on the contact surface of the molecule when used as drug in the aqueous environment such as in the human body and this can help in drug delivery design.

A clearer understanding of the molecular properties of prodigiosin has been seen and these properties can be used to understand how prodigiosin may be used in other applications. As a pyrrole molecule with conjugate bonding system, polymerization is foreseen for the prodigiosin molecule as this may lead to the production of an electrically conducting polymer from it.

## References

- [1] D. A. Karmaseh, "Effects of Prodigiosin on Breast Cancer Cell Viability," AUST, Abuja, 2016.
- [2] B. Peter and L. Bernard, "The World Cancer Report," WHO, 2008.
- [3] D. Cutierrez, "Cancer Facts and Figures," World Health Organization, 2008.
- [4] C. Daiz-Ruiz, B. Montaner and R. Perez-Tomas, "Prodigiosin Induces Cell Death," Department of Cell Biology, Cancer Biology Research Group, University of Barcelona, Barcelona.
- [5] L. G. Ferreira, R. N. dos Santos, G. Oliva and A. D. Andricopulo, "Molecular Docking and Structure-Based Drug Design Strategies," *Molecules*, vol. 20, pp. 13384-13421, 2015.
- [6] C. H. Lee, H. C. Huang and H. F. Juan, "Reviewing Ligand-Based Rational Drug Design: The Search for an Atp Synthase Inhibitor," *International Journal of Molecular Sciences*, vol. 12, pp. 5304-5318, 2011.
- [7] A. O. Isyaku, "STRUCTURAL, ELECTRONIC AND OPTICAL PROPERTIES OF Cu<sub>2</sub>SnS<sub>3</sub> SOLAR ABSORBER: A FIRST-PRINCIPLE DENSITY FUNCTIONAL THEORY INVESTIGATION," African University of Science and Technology, Abuja, 2019.
- [8] B. Hildebrandt, P. Wustin and W. P. Ceelen, *Carcinomatosis: A Multidisciplinary Approach*, New York: Springer, 2007.
- [9] B. Peter and L. Bernard, "The World Cancer Report," World Health Organization, 2008.
- [10] D. Irvine, L. Vincent, J. E. Graydon, N. Bubela and L. Thompson, "Cancer Nursing," vol. 17, no. 5, pp. 367-378, 1994.
- [11] C. D. Berg, H. Nawata, D. A. Bronzert and M. A. Lippman, "Altered estrogen and antiestrogen responsiveness in clonal variants of human breast cancer cells.," *Prog. Cancer Res. Ther.*, vol. 31, p. 161, 1984.
- [12] M. A. Blankenstein, M. S. Henkelman and J. G. M. Klijn, "Direct inhibitory effect of a luteinising hormone-releasing hormone agonist on MCF-7 human breast cancer cells," *Eur. J. Cancer Clin Oncol.*, vol. 21, p. 1493, 1985.

- [13] D. C. Mathers and D. Loncar, "Updated Projections of Global Mortality and Burden of Disease, 2002-2030; Data Sources, Methods and Results.," World Health Organization, 2005.
- [14] K. A. M. Eidne, C. A. Flanagan and R. P. Miller, "Gonadotrophin- releasing hormone binding sites in human breast cancer.," *Science*, vol. 229, p. 989, 1985.
- [15] W. B. Butler, P. J. Berlinski, R. K. Hillman, W. H. Kelsey and M. M. Toenniges, "Relation of in-vitro properties to tumorigenicity for a series of sublines of the human breast cancer cell line MCF-7," *Cancer Res.*, vol. 46, p. 6339, 1986.
- [16] P. Hohenberg and W. Kohn, "Inhomogeneous electron gas," *Physical Review*, vol. 136, no. 3B, p. 864, 1964.
- [17] W. Kohn and L. J. Sham, "Self-consistent equations including exchange and correlation effects," *Physical Review*, vol. 140, no. 4A, p. 1133, 1965.
- [18] J. P. Perdew and K. Schmidt, *Density Functional Theory and Its Applications to Materials*, Newyork: American Institute of Physics, 2001.
- [19] D. M. Ceperley, "Ground State of the Electron Gas by a Stochastic Method," *Physical Review Letters*, vol. 45, no. 7, p. 569, 1980.
- [20] J. P. Perdew, J. A. Chevary, S. H. Vosko, K. A. Jackson, M. R. Pederson, D. J. Singh and C. Fiolhais, "Atoms, molecules, solids, and surfaces: Applications of the generalized gradient approximation for exchange and correlation," *Physical Review B*, vol. 46, no. 11, pp. 6672-6675, 1992.
- [21] J. P. Perdew, K. Burke and M. Ernzerhof, "Generalized Gradient Approximation Made Simple," *Physical Review Letter*, vol. 77, no. 18, pp. 3865-3867, 1996.
- [22] A. D. Becke, "Densityfunctional thermochemistry. I. The effect of the exchangeonly gradient correction," *J. Chem. Phys.*, vol. 96, p. 2155, 1992.
- [23] P. Dufek, P. Blaha, V. Sliwko and K. Schwarz, "Generahzed-gradient-approximation description of band splittings in transition-metal oxides and Suorides," *Physical Review B*, vol. 49, no. 15, pp. 10171-10175, 1994.
- [24] A. D. Becke, "Density-functional thermochemistry. III. The role of exact exchange," *J. Chem. Phys.*, vol. 94, pp. 5648-5652, 1998.

- [25] P. J. Stephens and F. J. Devlin, "Ab Initio Calculation of Vibrational Absorption and Circular Dichroism Spectra Using Density Functional Force Fields," *The Journal of Physical Chemistry*, vol. 98, no. 45, pp. 11623-11627, 1994.
- [26] M. Belletete, J. F. Morin, M. Leclerc and G. Durocher, "A theoretical, spectroscopic and photophysical study of 2,7-carbazolenevinylene-based conjugated derivatives," *J. Phys. Chem.*, vol. 109A, pp. 6953-6940, 2005.
- [27] K. B. Benzon, M. Y. Sheena, H. T. Varghese, P. C. Yohannan, S. Armaković, S. J. Armaković, K. Pradhan, A. K. Nanda and A. C. Van, "Spectroscopic, DFT, molecular dynamics and molecular docking study of 1-butyl-2-(4-hydroxyphenyl)-4,5-dimethylimidazole 3-oxide based on DFT calculations," *Journal of Molecular Structure*, 2016.
- [28] R. G. Parr and R. G. Pearson, "Absolute hardness: companion parameter to absolute electronegativity," *Journal of the American Chemical Society*, vol. 105, no. 26, pp. 7512-7516, 1983.
- [29] G. Zhang and C. B. Musgrave, "Comparison of DFT methods of molecular orbital eigenvalue calculations," *Journal of Physical Chemistry A*, vol. 111, no. 8, pp. 1554-1560, 2007.
- [30] R. A. Costa, E. S. A. Junior, J. d. A. Bezerra, J. M. Mar, E. S. Lima, M. L. B. Pinheiro, D. V. C. Mendonça, G. B. P. Lopes, A. D. S. Branches and K. M. T. Oliveira, "Theoretical Investigation of the Structural, Spectroscopic, Electronic, and Pharmacological Properties of 4-Nerolidylcatechol, an Important Bioactive Molecule," *Journal of Chemistry*, vol. 2019, 2019.
- [31] T. A. Koopmans, "Über die zuordnung von welenfunktionen und eigenwerten zu den einzelnen elektroneneines atoms," *Physica 1*, pp. 105-112, 1993.
- [32] I. Fleming, *Frontier Orbitals and Organic Chemical Reactions*, London: Wiley, 1976.
- [33] N. Sharma, J. S. Dhau, A. Singh, A. Singh and A. K. Malik, "FT-IR, NMR, Molecular structure and HOMO-LUMO Studies of 3,5-Dimethyl-2-pyridylselenium Compounds by Density Functional Theory," *Research Gate*.
- [34] J.-i. Aihara, "Correlation found between the HOMO–LUMO energy separation and the chemical reactivity at the most reactive site for isolated-pentagon isomers of fullerenes," *Phys. Chem. Chem. Phys.*, vol. 2, pp. 3121-3125, 2000.



- [35] S. Arulmonzhi, M. Victor, R. Antony and J. Madhavan, "HOMO, LUMO analysis and first order hyperpolarizability of 2-amino-5-chloro benzophenone using computational methods," *Pelagia Research Library*, vol. 2, no. 6, pp. 158-163, 2011.
- [36] M. Alam, M. J. Alam, S. A. A. Nami, D.-U. Lee, M. Azam and S. Ahmad, "Computational and anti-tumor studies of 7a-Aza-B-homostigmast-5-eno [7a, 7-d] tetrazole-3b-yl chloride," *Journal of Molecular Structure*, vol. 1108, pp. 411-426, 2016.
- [37] A. Kumar, S. Kumar, S. Jain and P. Kumar, *Der Pharmacia Sinica*, vol. 2, pp. 92-104, 2010.
- [38] M. Alam and S. Park, "Molecular structure, spectral studies, NBO, HOMOeLUMO profile, MEP and Mulliken analysis of 3b,6b-dichloro-5a-hydroxy-5aecholestane," *Journal of Molecular Structure*, vol. 1159, pp. 33-45, 2018.
- [39] A. Pullman and B. Pullman, "Molecular electrostatic potential of the nucleic acids," *Quarterly Reviews of Biophysics*, vol. 14, no. 3, pp. 289-380, 1981.
- [40] J. S. Murray and K. Sen, *Molecular Electrostatic Potentials, Concepts and Applications*, Amsterdam: Elsevier, 1996.
- [41] E. Scrocco and J. Tomasi, "Electronic molecular structure, reactivity and intermolecular forces: heuristic interpretation by means of electrostatic molecular potential," *Adv. Quant. Chem*, vol. 11, pp. 161-193, 1978.
- [42] F. J. Luque, J. M. Lopez and M. Orozco, "Perspective on electrostatic interactions of a solute with a continuum, a direct utilization of ab initio molecular potentials for the prevision of solvent effects," *Theor. Chem.*, vol. 103, pp. 343-345, 2000.
- [43] S. Moro, M. Bacilieri, C. Ferrari and G. Spalluto, "Autocorrelation of molecular electrostatic potential surface properties combined with partial least squares analysis as alternative attractive tool to generate ligand based 3D-QSARs," *Curr. Drug Discovery Technol.*, vol. 2, pp. 13-21, 2005.
- [44] B. Kosar and C. Albayrak, "Spectrochim," *Acta A*, vol. 78, pp. 160-167, 2011.
- [45] C. K. Bagdassarian, V. L. Schramm and S. D. Schwartz, "Molecular Electrostatic Potential Analysis for Enzymatic Substrates, Competitive Inhibitors, and Transition-State Inhibitors," *J. Am. Chem. Soc.*, vol. 118, pp. 8825-8836, 1996.

- [46] S. R. Gadre and P. K. Bhadane, "Electrostatic Potentials of Atoms, Ions and Molecules," *Electrostatics in Chemistry*, 40-51 May 1999.
- [47] J. D. Westbrook, R. M. Levy and K. Krogh-Jespers, "Molecular Electrostatic Potentials and Partial Atomic Charges from Correlated Wave Functions: Applications to the Electronic Ground and Excited States of 3-Methylindole," *Journal of Computational Chemistry*, vol. 13, no. 8, pp. 979-989, 1992.
- [48] B. Lee and F. M. Richards, "The Interpretation of Protein Structures: Estimation of Static Accessibility," *J. Mol. Biol.*, vol. 55, pp. 379-400, 1971.
- [49] T. Ooi, M. Oobatake, G. Nmmethy and H. A. Scheraga, "Accessible surface areas as a measure of the thermodynamic parameters of hydration of peptides," *Proc. Natl. Acad. Sci. USA*, vol. 84, pp. 3086-3090, 1987.
- [50] J. Weiser, P. S. Shenkin and C. W. Still, "Approximate Solvent-Accessible Surface Areas from Tetrahedrally Directed Neighbor Densities," *Biopolymer*, vol. 50, pp. 373-380, 1999.
- [51] R. Adamczak, A. Porollo and J. Meller, "Combining Prediction of Secondary Structure and Solvent Accessibility in Proteins," *PROTEINS: Structure, Function, and Bioinformatics*, vol. 59, pp. 467-475, 2006.
- [52] K. V. Klenin, F. Tristram, T. Strunk and W. Wenzel, "Derivatives of Molecular Surface Area and Volume: Simple and Exact Analytical Formulas," *J. Comput. Chem.*, vol. 32, pp. 2647-2653, 2011.
- [53] G. Kresse and J. Hafner, "Ab initio molecular dynamics for liquid metals," *Phys. Rev. B: Condens. Matter Mater. Phys.*, vol. 47, p. 558, 1993.
- [54] G. Kresse and J. Hafner, "Ab initio molecular-dynamics simulation of the liquid-metal–amorphous-semiconductor transition in germanium," *Phys. Rev. B: Condens. Matter Mater. Phys.*, vol. 49, p. 14251–14269, 1994.
- [55] G. Kresse and J. Furthmüller, "Efficient iterative schemes for ab initio total-energy calculations using a plane-wave basis set," *Phys. Rev. B: Condens. Matter Mater. Phys.*, vol. 54, p. 11169–11186, 1996.
- [56] P. E. Blöchl, "Projector augmented-wave method," *Phys. Rev. B: Condens. Matter Mater. Phys.*, vol. 50, p. 17953, 1994.

- [57] G. Kresse and D. Joubert, "From ultrasoft pseudopotentials to the projector augmented-wave method," *Phys. Rev. B: Condens. Matter Mater. Phys.*, vol. 59, p. 1758, 1999.
- [58] J. P. Perdew, K. Burke and M. Ernzerhof, "Generalized Gradient Approximation Made Simple," *Phys. Rev. Lett.*, vol. 78, p. 1396, 1997.
- [59] J. P. Perdew, K. Burke and M. Ernzerhof, "Generalized Gradient Approximation Made Simple," *Phys. Rev. Lett.*, vol. 77, p. 3865–3868, 1996 .
- [60] S. Grimme, J. Antony, S. Ehrlich and S. Krieg, "A consistent and accurate ab initio parametrization of density functional dispersion correction (DFT-D) for the 94 elements H-Pu," *J. Chem. Phys.*, vol. 132, p. 154104, 2010.
- [61] R. S. Mulliken, "Electronic population analysis on LCAO-MO molecular wavefunction," *J. Chem. Phys.*, vol. 23, pp. 1833-1840, 1955.
- [62] M. Belletete, J. F. Morin, M. Leclerc and G. Durocher, "A theoretical, spectroscopic and photophysical study of 2,7-carbazolenevinylene-based conjugated derivatives," *J. Phys. Chem.*, vol. 109A, pp. 6953-6958, 2005.
- [63] T. Abbaz, A. Bendjeddou and D. Villemin, "Molecular structure, HOMO, LUMO, MEP, natural bond orbital analysis of benzo and anthraquinodimethane derivatives," *PHARMACEUTICAL AND BIOLOGICAL EVALUATIONS*, vol. 5, pp. 27-39, 2018.
- [64] R. J. Parr, L. V. Szentpaly and S. Liu, "Electropilicity Index," *J. Am. Chem. Soc.*, vol. 121, pp. 1922-924, 1999.
- [65] J. F. Luque, M. J. Lopez and M. Orozco, "Perspective on electrostatic interactions of a solute with a continuum, a direct utilization of ab initio molecular potentials for the prevision of solvent effects," *Theor. Chem. Acc.*, vol. 103, pp. 343-345, 2000.